Greenland Ice Sheet Mass Balance Reconstruction. Part I: Net Snow Accumulation (1600–2009)

JASON E. BOX,* NOEL CRESSIE,+ DAVID H. BROMWICH,* JI-HOON JUNG,* MICHIEL VAN DEN BROEKE,# J. H. VAN ANGELEN,# RICHARD R. FORSTER,@ CLEMENT MIÈGE,@ ELLEN MOSLEY-THOMPSON,* BO VINTHER,& AND JOSEPH R. MCCONNELL**

* *Byrd Polar Research Center, and Department of Geography, The Ohio State University, Columbus, Ohio*
+ *Department of Statistics, The Ohio State University, Columbus, Ohio, and National Institute for Applied Statistics Research Australia, University of Wollongong, Wollongong, New South Wales, Australia*
# *Institute of Marine and Atmospheric Research, Utrecht University, Utrecht, Netherlands*
@ *Department of Geography, University of Utah, Salt Lake City, Utah*
& *Centre for Ice and Climate, Niels Bohr Institute, Copenhagen, Denmark*
** *Desert Research Institute, Reno, Nevada*

(Manuscript received 20 June 2012, in final form 14 November 2012)

ABSTRACT

Ice core data are combined with Regional Atmospheric Climate Model version 2 (RACMO2) output (1958–2010) to develop a reconstruction of Greenland ice sheet net snow accumulation rate, $\hat{A}_t(G)$, spanning the years 1600–2009. Regression parameters from regional climate model (RCM) output regressed on 86 ice cores are used with available cores in a given year resulting in the reconstructed values. Each core site's residual variance is used to inversely weight the cores' respective contributions. The interannual amplitude of the reconstructed accumulation rate is damped by the regressions and is thus calibrated to match that of the RCM data. Uncertainty and significance of changes is measured using statistical models.

A 12% or 86 Gt yr^{-1} increase in ice sheet accumulation rate is found from the end of the Little Ice Age in ~1840 to the last decade of the reconstruction. This 1840–1996 trend is 30% higher than that of 1600–2009, suggesting an accelerating accumulation rate. The correlation of $\hat{A}_t(G)$ with the average surface air temperature in the Northern Hemisphere ($SATNH_t$) remains positive through time, while the correlation of $\hat{A}_t(G)$ with local near-surface air temperatures or North Atlantic sea surface temperatures is inconsistent, suggesting a hemispheric-scale climate connection. An annual sensitivity of $\hat{A}_t(G)$ to $SATNH_t$ of 6.8% K^{-1} or 51 Gt K^{-1} is found.

The reconstuction, $\hat{A}_t(G)$, correlates consistently highly with the North Atlantic Oscillation index. However, at the 11-yr time scale, the sign of this correlation flips four times in the 1870–2005 period.

1. Introduction

It is well known that ice sheet mass balance exerts a significant influence on global mean sea level. This mass balance is between net snow accumulation and mass losses from surface and basal melting and from glacier ice discharge. Given that net snow accumulation is the only net mass input, it is important for ice sheet mass balance models to have accurate depictions of the spatial and temporal ice sheet accumulation rates. Another important question is whether the Greenland ice sheet is accumulating more snow due to climate warming.

Greenland ice sheet accumulation maps have been based on multiyear average spatial distributions of ice/firn cores and coastal precipitation records (Ohmura and Reeh 1991; Calanca et al. 2000; Bales et al. 2001a,b; Cogley 2004; Bales et al. 2009). McConnell et al. (2001) mapped the annual time variation of accumulation for the southern ice sheet, finding high spatial and temporal variability. Global climate model simulations of precipitation around Greenland (e.g., Ohmura et al. 1996; Thompson and Pollard 1997; Wild and Ohmura 2000) produce insight into possible future accumulation increases but are challenged in resolving extremes over the narrow southeastern ice sheet (e.g., Walsh et al.

Corresponding author address: Jason E. Box, Oester Voldgade 10, DK-1350 Copenhagen K, Denmark.
E-mail: jbox.greenland@gmail.com

DOI: 10.1175/JCLI-D-12-00373.1

2008). Atmospheric reanalyses are found to capture snow accumulation temporal variability over Greenland, when compared with ice cores (Hanna et al. 2001, 2006, 2011). Higher-resolution regional climate models have been used to examine Greenland accumulation (e.g., Dethloff et al. 2002; Kiilsholm et al. 2003; Box et al. 2004, 2006; Box 2005; Fettweis et al. 2008; Aðalgeirsdóttir et al. 2009; Ettema et al. 2009; Rae et al. 2012). Accurate representation of model terrain elevation is essential in realistic simulation of accumulation (Box and Rinke 2003). Increasing model horizontal resolution shifts peak accumulation closer to the coast (Lucas-Picher et al. 2011).

Burgess et al. (2010) added spatial and temporal resolution to Greenland ice sheet accumulation through a fusion of firn cores, precipitation data from meteorological stations, and precipitation rate calculations from the fifth-generation Pennsylvania State University–National Center for Atmospheric Research Mesoscale Model (MM5) modified for polar climates (Polar MM5). The highest variability in accumulation rate is found on the southeast ice sheet and at elevations where few ice cores have been drilled. In effect, an area corresponding with roughly half of the ice sheet accumulation total is solely represented by the climate model. Ohmura and Reeh (1991), Chen et al. (1997), and Hutterli et al. (2005) identify an important relationship between Greenland precipitation and cyclonic activity. Alternating eastern versus western slope accumulation variability was identified by Burgess et al. (2010) and is consistent with Rogers et al. (2004), who distinguish lee cyclones from ''Icelandic'' cyclones, as they produce opposite precipitation effects over the ice sheet. Regional accumulation trends are found to be temporally and spatially variable (Mosley-Thompson et al. 2001), as is the influence of North Atlantic atmospheric circulation on accumulation (Mosley-Thompson et al. 2005).

The 1958–2007 average ice sheet annual accumulation rate after Burgess et al. (2010) was found to be ~70 Gt larger than for estimates obtained previously, the discrepancy being largely due to Polar MM5 data including regions of orographic precipitation enhancement around the ice sheet periphery. The discrepancy in the southeast was also noted by Ettema et al. (2009).

Wake et al. (2009) incorporated snow accumulation reconstruction, based on the Box et al. (2009) approach for surface air temperature reconstruction, to estimate the time variation of whole ice sheet accumulation since 1866. Taking the baseline period 1961–90 to represent a stable climate and mass balance period, Wake et al. found an increase in cumulated surface mass balance over much of the southern and western ice sheet accumulation areas. Studies indicate some evidence of increasing ice sheet snow accumulation rate since the late 1950s (Hanna et al. 2005, 2011).

To better understand the spatial and temporal variability of Greenland ice sheet accumulation, the reconstruction methodology of Box et al. (2009) is refined and applied to a set of 86 ice core accumulation records. Our analysis produces a spatial grid of annually resolved accumulation reconstruction spanning the period of available core data, here year 1600 and onward. The fundamental goal is to reconstruct the spatial and temporal patterns of net snow accumulation, especially before 1958 when high-resolution regional climate model output remains unavailable. Uncertainty is quantified here using a statistical analysis of residuals from the regressions upon which the reconstruction is based. The time dependence of the net snow accumulation is reassessed for the ice sheet as a whole and regionally. The regression model is used to establish the certainty in the reconstruction. The resulting accumulation reconstruction is compared with regional and hemispheric climate parameters.

2. Data

a. Snow accumulation from ice cores

Annually resolved accumulation rate data were obtained from 86 ice cores (Fig. 1; Table 1). The accuracy of these data is affected by wind-driven snow redistribution, melt and vapor diffusional vertical redistribution of chemical species, dating errors, and measurement uncertainties (Mosley-Thompson et al. 2001). The number of ice core records available for the reconstruction in year 1600 is 6. By year 1700, the number of available cores is 13; by 1750 it is 21 cores; by 1800 it is 31 cores; by 1850 it is 34 cores; and by 1900 it is 36 cores. The number increases to a maximum of 72 cores during 1986–88 (Fig. 2). While there are 86 cores available during the period 1600–2009, many of them are for shorter periods. The spatial distribution of the ice core dataset is broad, providing some data in different topographic basins, even before year 1800 (Fig. 1).

b. Regional climate model output

1) POLAR MM5

Output from MM5, modified for use in polar regions (Bromwich et al. 2001; Cassano et al. 2001), is one of two climate model outputs used in this study. In the 24-km horizontal grid resolution model configuration used here, Polar MM5 is reinitialized once per month and updated every 6 h at the lateral boundaries using

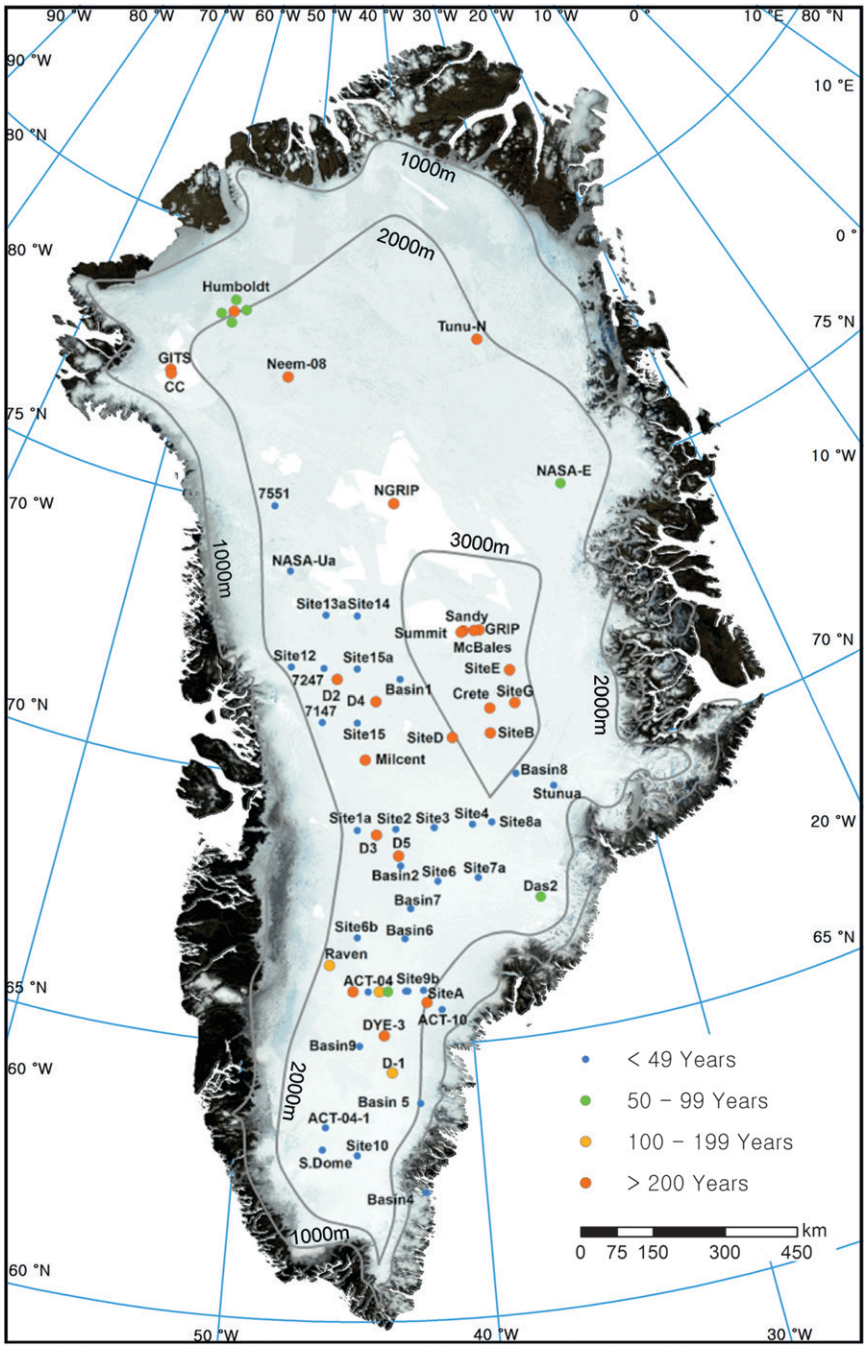

FIG. 1. Annually resolved firn/ice cores used in this study. The color of map markers indicates the number of years in the ice core record.

2.5° horizontal resolution 40-yr European Centre for Medium-Range Weather Forecasts (ECMWF) Re-Analysis (ERA-40) data for 1958–2002. For 2002–08, 12-hourly ECMWF operational analyses are used to initialize Polar MM5. Thus, these data span a 51-yr period, 1958–2008.

We used 3-hourly model output to produce annual total precipitation grids. Precipitation was converted into net snow accumulation rate by warping the grid through average ice core values, after Burgess et al. (2010), implicitly accounting for the 10%–20% mass loss from surface and blowing snow H_2O gas flux (Box and

TABLE 1. Annually resolved ice core-derived accumulation data summary. The variable precision of site coordinates reflects precision reported in the data sources.

Site name	Latitude (°N)	Longitude (°W)	Time span	Time span (No. years)	Source
7147	71	47	1974–96	23	Program for Arctic Regional Climate Assessment (PARCA), McConnell et al. (2000)
7247	72	47	1974–96	23	PARCA, McConnell et al. (2000)
7551	75	51	1965–96	32	PARCA, McConnell et al. (2000)
ACT-04–1	63.5	46.3	1958–2003	46	Hanna et al. (2011)
ACT-04–2	66	45.2	1772–2003	232	Hanna et al. (2011)
ACT-04–3	66	43.6	1838–2003	166	Hanna et al. (2011)
ACT-04–4	66	42.8	1979–2003	25	Hanna et al. (2011)
ACT-10a	65.63	41.2	1985–2009	25	Forster et al. (2010)
ACT-10b	65.77	41.87	1980–2009	30	Forster et al. (2010)
ACT-10c	66	42.72	1973–2009	37	Forster et al. (2010)
ACT-11b	66.22	39.57	1969–2010	42	Forster et al. (2010)
ACT-11c	66.34	41.77	1973–2010	38	Forster et al. (2010)
ACT-11d	66.48	46.31	1761–2010	250	Forster et al. (2010)
Basin1	71.8	42.44	1976–2002	27	PARCA, Hanna et al. (2006)
Basin2	68.32	42.83	1980–2002	23	PARCA, Hanna et al. (2006)
Basin4	62.31	46.3	1973–2002	30	PARCA, Hanna et al. (2006)
Basin5	63.93	42.35	1964–2002	39	PARCA, Hanna et al. (2006)
Basin6	66.96	42.75	1983–2002	20	PARCA, Hanna et al. (2006)
Basin7	67.52	42.41	1983–2002	20	PARCA, Hanna et al. (2006)
Basin8	69.84	36.4	1957–2002	46	PARCA, Hanna et al. (2006)
Basin9	65	44.9	1956–2002	47	PARCA, Hanna et al. (2006)
CC	77.17	61.13	1762–1974	213	Clausen and Hammer (1988)
CC2	77.17	61.13	1839–1974	136	Clausen and Hammer (1988)
Crete	71.12	37.32	552–1973	1422	Andersen et al. (2006)
D1	64.5	43.5	1848–1997	150	PARCA, Mosley-Thompson et al. (2005)
D2	71.8	46.2	1781–1997	217	PARCA, Mosley-Thompson et al. (2005)
D3	68.9	44	1740–1997	258	PARCA, Mosley-Thompson et al. (2005)
D4	71.4	43.9	1738–2002	265	Banta and McConnell (2007)
D5	68.5	42.9	1700–2002	303	Banta and McConnell (2007)
DYE-3–18C	65.18	43.83	1777–1976	200	Mayewski et al. (1990); Vinther et al. (2010)
DYE-3–20D	65.18	43.83	1775–1983	209	Mayewski et al. (1990); Vinther et al. (2010)
Das1	66	44	1908–2002	95	Banta et al. (2008)
Das2	67.5	36.1	1936–2002	67	Banta et al. (2008)
GITS-1	77.1	61	1964–95	32	PARCA, Mosley-Thompson et al. (2005)
GITS-2	77.1	61	1745–1995	251	PARCA, Mosley-Thompson et al. (2005)
GRIP	72.58	37.32	1–1979	1979	Andersen et al. (2006)
GRIP89S1	72.58	37.64	919–1988	1070	White et al. (1997); Vinther et al. (2010)
GRIP89S2	72.58	37.64	1772–1986	215	White et al. (1997); Vinther et al. (2010)
GRIP91S1	72.58	37.64	1728–1988	261	White et al. (1997); Vinther et al. (2010)
GRIP92S1	72.58	37.64	1623–1986	364	White et al. (1997); Vinther et al. (2010)
GRIP93S1	72.58	37.64	1063–1990	928	White et al. (1997); Vinther et al. (2010)
Hum.E	78.45	57.96	1929–94	66	PARCA, McConnell et al. (2000)
Hum.Main	78.53	56.83	1700–1992	293	PARCA, McConnell et al. (2000)
Hum.N	78.75	56.83	1927–94	68	PARCA, McConnell et al. (2000)
Hum.S	78.32	56.83	1924–94	71	PARCA, McConnell et al. (2000)
Hum.W	78.6	55.7	1924–94	71	PARCA, McConnell et al. (2000)
Humboldt	78.53	56.83	1699–1993	295	PARCA, McConnell et al. (2000)
McBales	72.55	38.31	1700–1999	300	Banta and McConnell (2007)
Milcent	70.3	44.55	1174–1966	793	Andersen et al. (2006)
N.DYE-2	66	44.5	1978–96	19	PARCA
N.DYE-3	66	44.5	1976–96	21	PARCA
NASA-Ea	75	30	1931–96	66	PARCA
NASA-Eb	75	30	1968–96	29	PARCA
NASA-Ua	73.8	49.5	1965–93	29	PARCA, Mosley-Thompson et al. (2005)
NEEM-2008-S3	77.45	51.06	1746–2000	255	McConnell

TABLE 1. (*Continued*)

Site name	Latitude (°N)	Longitude (°W)	Time span	Time span (No. years)	Source
NGRIP	75.1	42.32	187–1995	1809	Andersen et al. (2006)
Raven-DO18	66.48	46.28	1864–1995	132	Mosley-Thompson et al. (2005)
Raven-Dust	66.48	46.28	1864–1995	132	Mosley-Thompson et al. (2005)
S.Dome a	63.1	46.4	1978–96	19	PARCA, McConnell et al. (2000)
S.Dome b	63.1	46.4	1986–96	11	PARCA, McConnell et al. (2000)
S.Tunu a	69.5	34.5	1975–96	22	PARCA, McConnell et al. (2000)
S.Tunu b	69.5	34.5	1987–96	10	PARCA, McConnell et al. (2000)
S.Tunu c	69.5	34.5	1987–96	10	PARCA, McConnell et al. (2000)
Sandy	72.6	38.3	1753–2002	250	PARCA
Site 10	63	45	1977–97	21	PARCA
Site 12	72	49	1986–97	12	PARCA
Site 13a	73	47	1980–97	18	PARCA
Site 14	73	45	1975–97	23	PARCA
Site 15	71	45	1984–97	14	PARCA
Site 15a	72	45	1986–97	12	PARCA
Site 1a	69	45	1977–97	21	PARCA
Site 2	69	43	1976–97	22	PARCA
Site 3	69	41	1985–97	13	PARCA
Site 4	69	39	1982–97	16	PARCA
Site 6	68	41	1986–97	12	PARCA
Site 6b	67	45	1984–97	14	PARCA
Site 7a	68	39	1984–97	14	PARCA
Site 8a	69	38	1983–97	15	PARCA
Site 9b	66	42	1981–97	17	PARCA
SiteA	70.63	35.82	1623–1983	361	Clausen and Hammer (1988); Vinther et al. (2010)
SiteB	70.65	37.48	1717–1982	266	Clausen and Hammer (1988); Vinther et al. (2010)
SiteD	70.64	39.62	1767–1982	216	Clausen and Hammer (1988); Vinther et al. (2010)
SiteE	71.76	35.85	1722–1982	261	Clausen and Hammer (1988); Vinther et al. (2010)
SiteG	71.15	35.84	1777–1983	207	Clausen and Hammer (1988); Vinther et al. (2010)
Summit-Zoe-10	72.58	38.46	1743–2010	268	McConnell
Tunu-N	78.02	33.99	1699–1994	296	McConnell

Steffen 2001; Box et al. 2006; Mernild et al. 2008; Ettema et al. 2009; Lenaerts et al. 2012a,b).

2) RACMO2

The Regional Atmospheric Climate Model version 2 (RACMO2) (Van Meijgaard et al. 2008) combines the dynamical parameterizations from the High-Resolution Limited-Area Model (HIRLAM; Undén et al. 2002) with the physics package of the ECMWF model. The polar version of RACMO2 has previously been used to assess the climate and surface mass balance of the ice sheets of Antarctica (Van de Berg et al. 2006; Lenaerts and van den Broeke 2012) and Greenland (Ettema et al. 2009; Van den Broeke et al. 2009; Van Angelen et al. 2011). The model has an interactive snowpack that allows for meltwater retention, refreezing, and runoff. The drifting snow scheme of Déry and Yau (1999) is interactively coupled to the RACMO2 boundary layer scheme to calculate drifting snow transport and sublimation (Lenaerts et al. 2010). Every 6 h, RACMO2 is forced at its lateral boundaries by ECMWF reanalyses, ERA-40 (1960–88) and the ECMWF Interim Re-Analysis (ERA-Interim; 1989–2010). Thus, these data span a 51-yr period, 1960–2010. These forcings are interpolated toward true model resolution (11 km) in the relaxation zone at the edges of the 11-km domain. Accumulation data from RACMO2 used here are set equal to precipitation minus surface water vapor flux (i.e., evaporation/sublimation).

c. Interpolation

The accumulation rate grids for Polar MM5 and RACMO2 are resampled to a 5-km equal area grid using bilinear interpolation (http://nsidc.org/data/modis/ms2gt/). The finer grid facilitates colocating of point data for model error assessment and calibration. Choosing a finer resolution grid than 5 km was excluded because of limits in available computational resources.

d. Ice sheet mask

Classification of the grid cells as permanent ice, land, ocean, and mixed ''pixels'' is made using 1.25-km

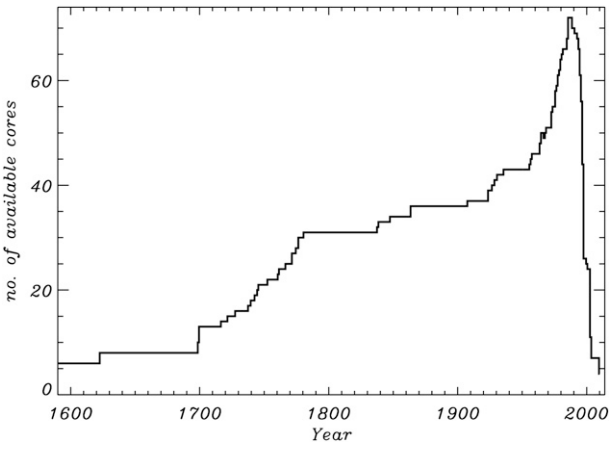

FIG. 2. Time dependence of ice core data availability in this study.

resolution June–August National Aeronautics and Space Administration (NASA) Moderate Resolution Imaging Spectroradiometer (MODIS) bands 1–4 and 6 cloud-free imagery from 2006. The surface is considered permanent ice if surface reflectance exceeds 0.3 and if the Normalized Difference Vegetation Index (NDVI) is less than 0.1. When the 1.25-km grid is interpolated to 5 km using a ''nearest neighbor'' basis to quantify how much mixing of the grid cells by land takes place, it is possible to define a ''fuzzy'' mask that quantifies the mixing of land and ice using a value between 0 and 1. As such, selection of a mask threshold to represent the average case of permanent ice partially addresses the subgrid issue while maintaining the ability to accurately determine the mass flux. Based on this classification, our best estimate of the permanent ice covered area tuned to match permanently glaciated areas reported by Kargel et al. (2011) corresponds with mask values greater than or equal to 0.587, resulting in an area of 1.824×10^6 km^2. Non-ice-sheet grid cells are excluded from the reconstruction. There are 72 974 grid cells counted as glaciated. Approximately 2496 of these grid cells are isolated from the inland ice sheet, totaling 62 393 km^2. Accumulation totals presented in this work are for the total Greenland ice area and do not partition the peripheral glaciers and ice caps.

e. Regional climate records

Northern Hemisphere surface air temperatures (SAT) (Hansen et al. 1999, 2010), Greenland ice sheet averaged surface air temperature data after Box et al. (2009), North Atlantic sea surface temperature (SST) (Rayner et al. 2006), and North Atlantic Oscillation (NAO) index (Hurrell 1995) data are available with time spans that enable examining potential interactions with accumulation rates at interdecadal time scales. At the time of this study, the common period for these datasets is 126 years (1880–2005).

3. Methods

a. Regression-based reconstruction in space and time

The reconstruction method used in this study employs least squares regression parameters of the annual regional climate model (RCM) net snow accumulation rates versus annually resolved ice sheet snow accumulation rates from firn/ice cores. An overlap of at least 15 years is selected as the minimum acceptable sample size for a regression. Data from the two RCMs, Polar MM5 and RACMO2, are compared. The individual time series at each grid cell in the RCM Greenland ice sheet domain is regressed on the concomitant time series from each core. For each ice core site, grids covering the ice sheet and containing the regression summaries—that is, number of (x, y) pairs, intercept, slope, correlation, sum of squares of the regressor (i.e., core) values, and residual variance—are stored for later use by the reconstruction algorithm. All regressions are carried out assuming errors are spatially and temporally independent; future research may investigate the role of spatiotemporal statistics.

The RCM data are set as the explanatory (i.e., dependent, or y) variable, and the in situ records from ice cores are set as the driver (i.e., independent, or x) of the reconstruction. This regression approach exploits the respective strengths of the data: the complete spatial coverage of the climate model output and the generally longer duration of the ice core records. It is similar to the approach that Box et al. (2009) used for surface air temperature reconstruction. However, rather than using the Box et al. (2009) ''winner take all'' approach, multiple available cores are used simultaneously, with each site's variance of the estimated mean accumulation used to inversely weight their respective contribution to the reconstructed value.

We are estimating a mean accumulation, $\mu_t(s)$, indexed by year t and grid cell s that corresponds to rectangular grid coordinates i and j. The 5-km grid used in this case has up to 301 grid cells in the i direction (nominally east–west) and 561 cells in the j direction (nominally north–south). See section 2d for grid cell count and ice area.

A climate model produces net snow accumulation values, $Y_t(s)$. Let the true accumulation, $A_t(s)$, have mean $\mu_t(s)$ and assume that the climate model gives unbiased estimates (E); that is,

$$E[Y_t(s)] = E[A_t(s)] = \mu_t(s).$$

For a given t (e.g., $t = 1750$) and a given s (e.g., a grid cell at the ice sheet topographic summit), the estimate

$\hat{\mu}_t(s)$ is made up of $k = 1, \ldots, 86$ regression estimates, corresponding to a regression of the pairs

$$[x_u(s_k), Y_u(s)]; \quad u \in T_k,$$

where T_k is the collection of years at the kth core that overlap with the years that the climate model output is available. Here, for $k = 1, \ldots, 86$, s_k is the location of the kth core, $x_u(s_k) \equiv c_u(s_k)$ for $u \in T_k$, and $\{c_t(s_k)\}$ are all the core values at the kth core. In other words, we *rename* the most recent core values using the more conventional letter x.

Now, we fit the linear model,

$$Y_u(s) = \alpha(s)_k + \beta(s)_k x_u(s_k) + \varepsilon_u(s)_k; \quad u \in T_k,$$

where u varies over $|T_k| = N_k$ years during the period 1960–2010 for RACMO2 and $\in$ means "belongs to." That is, there are $N_k \leq 51$ x–y points to which a regression is fitted. This results in estimates $\hat{\alpha}(s)_k$ and $\hat{\beta}(s)_k$, where the subscript k outside of $\hat{\alpha}(s)$ and $\hat{\beta}(s)$ is used to denote the use of the kth core in the regression. Then the estimate of the mean, based on the kth regression, is

$$\hat{\mu}(s)_k = \hat{\alpha}(s)_k + \hat{\beta}(s)_k c_t(s_k),$$

recalling that $c_t(s_k)$ is the core value at time t at the kth core. For example, $t = 1750$, s is a grid cell at the ice sheet topographic summit, and $k = 5$ (i.e., the fifth ice-core, ACT-04–02).

Assuming temporal independence, compute

$$\mathrm{var}[\hat{\mu}(s)_k] = S_t(s)_k^2 \left\{ \frac{1}{N_k} + \frac{[c_t(s_k) - \bar{x}(s_k)]^2}{\sum_{u \in T_k} [x_u(s_k) - \bar{x}(s_k)]^2} \right\},$$

where

$$\bar{x}(s_k) = \frac{1}{N_k} \sum_{u \in T_k} x_u(s_k), \quad \text{and}$$

$$S_t(s)_k^2 = \frac{1}{N_k - 2} \sum_{u \in T_k} [Y_u(s) - \hat{\alpha}(s)_k - \hat{\beta}(s)_k x_u(s_k)]^2.$$

The combined estimate of $\mu_t(s)$ from all 86 regressions is

$$\hat{\mu}_t(s) \equiv \sum_{k=1}^{86} w_t(s)_k \hat{\mu}_t(s)_k,$$

where the weighting of each core's contribution to the estimated mean is

$$w_t(s)_k \equiv \frac{1/\mathrm{var}[\hat{\mu}_t(s)_k]}{\sum_{l=1}^{86} 1/\mathrm{var}[\hat{\mu}_t(s)_l]}.$$

Thus, $\hat{\mu}_t(s)$ is a function of all cores, $\{c_t(s_1), \ldots, c_t(s_{86})\}$, which allows all core measurements to influence the estimate: Cores whose regressions do not fit very well, characterized by large $\mathrm{var}[\hat{\mu}(s)_k]$, receive a small weight in the combined estimate, $\hat{\mu}_t(s)$.

The variance of $\hat{\mu}_t(s)$ is

$$\sigma_t(s)^2 = \frac{1}{\sum_{l=1}^{86} 1/\mathrm{var}[\hat{\mu}_t(s)_l]},$$

the standard deviation is $\sigma_r(s)$, and an approximate 95% confidence interval is

$$\hat{\mu}(s) \pm 1.96\sigma_t(s).$$

The estimates, $\hat{\mu}_t(s)$, can be combined over s and/or over t. For example, aggregate all s over the ice sheet: The total snow accumulation at time t over all of Greenland is $A_t(G) \equiv \sum_{s \in G} \mu_t(s) a$, where $G \equiv$ Greenland and a is the 5-km-resolution grid cell area of 2.5×10^7 m^2. We estimate this with

$$\hat{A}_t(G) \equiv \sum_{s \in \mathrm{G}} \hat{\mu}_t(s) a.$$

Then, assuming spatial independence,

$$\sigma_t(G)^2 \equiv \mathrm{var}[\hat{A}_t(G)] = \sum_{s \in G} \sigma_t(s)^2 a^2,$$

where $\sigma_t(s)^2$ is given above. The standard deviation is $\sigma_r(G)$, and an approximate 95% confidence interval is

$$\hat{A}_t(G) \pm 1.96\sigma_t(G).$$

Suppose we wish to consider two times, $t0$ and $t1$, and we test the hypotheses

$$H_0: A_{t1}(G) - A_{t0}(G) = 0 \quad \text{versus}$$
$$H_1: A_{t1}(G) - A_{t0}(G) \neq 0,$$

recalling that $A_t(G) \equiv \sum_{s \in G} \mu_t(s) a$ is the total accumulation over Greenland at time t. We estimate $A_t(G)$ with $\hat{A}_t(G)$. Hence, we can test the hypotheses at the $\alpha = 0.05$ significance level as follows: If the confidence interval,

$$\hat{A}_{t1}(G) - \hat{A}_{t0}(G) \pm 1.96[\sigma_{t1}(G)^2 + \sigma_{t0}(G)^2]^{1/2},$$

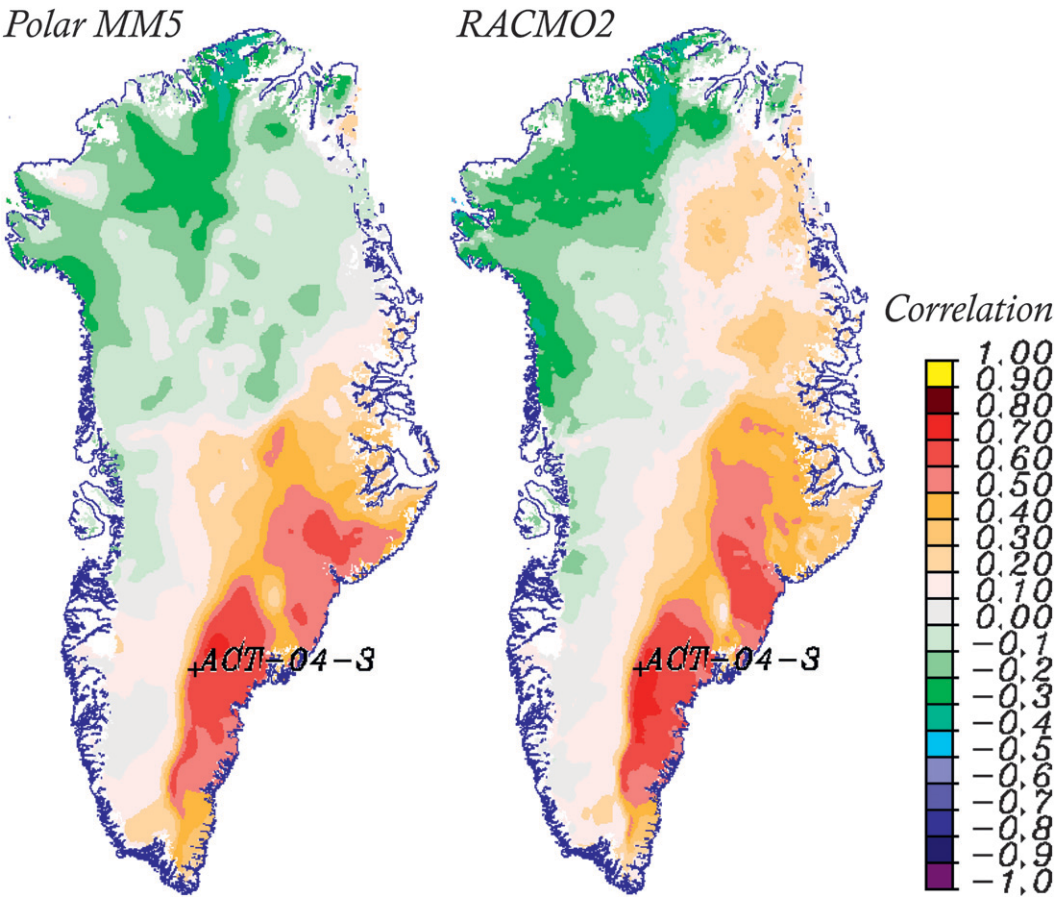

FIG. 3. Examples of the spatial correlation pattern between ice core accumulation rate and accumulation simulated by regional climate models over the 1960–2003 period.

contains zero, we accept H_0. Otherwise, we conclude that there is a significant difference between the mean accumulation at ice sheet grid cells at time $t1$ compared to that at time $t0$.

The p value is the probability that the test statistic is more extreme than its observed value, calculated assuming H_0 is true. Thus, $(1 - p)100\%$ expresses a "level of confidence" that the trend is nonzero.

b. Time series analysis

To identify and illustrate interdecadal fluctuations, and because individual years have greater uncertainty, Gaussian-weighted running-mean filters are used to smooth the time series. We consider 11- and 21-yr filters with 2.5- and 4-yr standard deviations, respectively. For the 5 or 10 yr (respectively) of the time series' beginning or end, the tail of the Gaussian filter (or "boxcar") is truncated by one year for each year approaching the end of the series, until the sample represents a trailing (leading) mean of 5 or 10 yr at the end (beginning) of the time series, respectively. In the 21-yr case, the standard deviation of 4 yr and the interval of 21 yr is chosen so that the filter includes a decade on either side of the time point of interest, and $^{20}/_{4} = 5$. The 11-yr smoothing is roughly consistent with that of the Andersen et al. (2006) "common record" from five accumulation records, hereafter ACR_t.

4. Results

a. Spatial correlation patterns

Examples of the spatial correlation patterns between a time series of accumulation for the ACT-04–03 ice core and those from the Polar MM5 and RACMO2 RCM simulations indicate typical distance–decay of correlation and negative correlation in leeward topographic basins (Fig. 3). The topographic antiphase correlations indicate the effects of storm track direction and orography (Rogers et al. 2004). For example, eastern coring sites capture a positive correlation signal along the eastern ice sheet and are often accompanied by negative correlation patterns west of the ice sheet topographic divide that indicate precipitation shadowing.

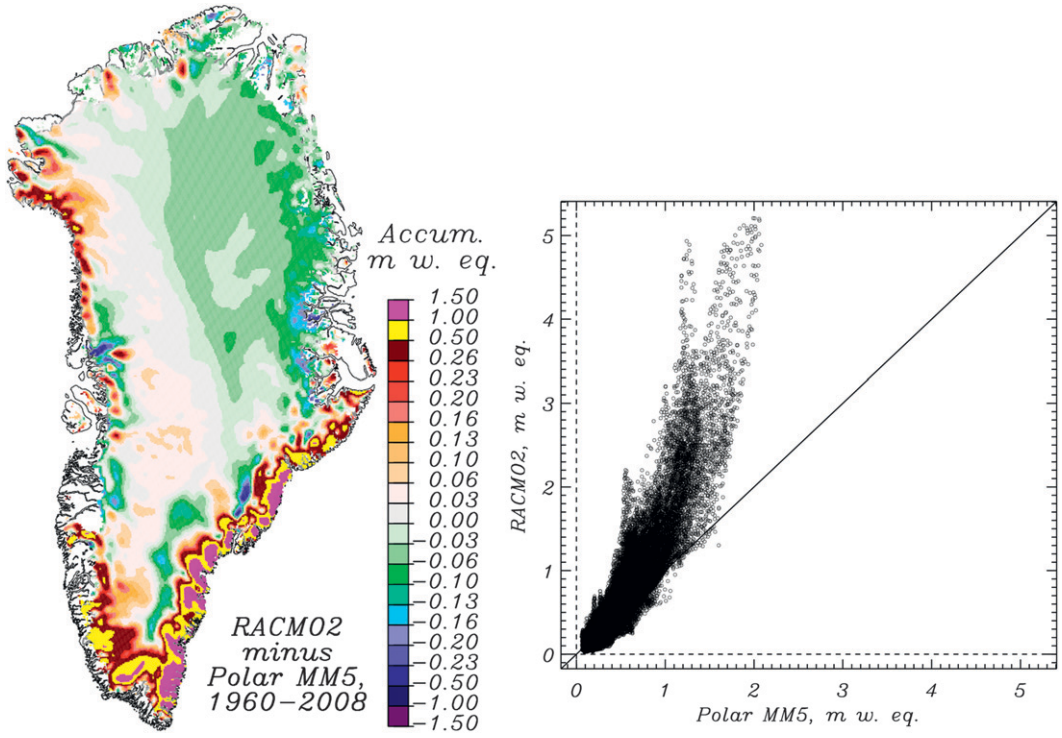

FIG. 4. (left) Spatial pattern of the difference in average RACMO2 and Polar MM5 ice sheet accumulation rates. (right) Scatterplot of RACMO2 and Polar MM5 accumulation rates.

RACMO2 data, which are output at 11-km horizontal resolution, contain more spatial detail than the Polar MM5 output at 24 km. In more cases than not, RACMO2 output also resulted in wider regions of positive correlation (Fig. 3). From local comparison with ice cores, RACMO2 interannual variability is 22% greater than Polar MM5. RACMO2 more often than not produces higher peak correlation than Polar MM5 (Fig. 3). There are several exceptions when Polar MM5 data produce higher peak correlation with core data. Adding the surface water vapor flux from evaporation and sublimation slightly increases the RACMO2 correlations in the majority of cases. Adding RACMO2 snow drift divergence introduces high-frequency spatial variability that reduces correlations and is left out of the reconstruction.

b. Accumulation magnitude

RACMO2 simulates higher accumulation than Polar MM5 (Fig. 4) along the ice sheet margin in the southeast and west. The fact that RACMO2 has higher spatial resolution (11 km) than Polar MM5 (24 km) means that it is able to better resolve localized peak accumulation features. Ettema et al. (2009) attribute the higher spatial resolution of RACMO2 as the reason it simulates higher precipitation and thus accumulation rates in these topographically enhanced precipitation regions. Shallow firn cores in the vicinity of peak accumulation areas confirm this result. While Polar MM5 also captures orographic peak accumulation, its 24-km resolution underpredicts the peaks. While reconstruction results are similar between RACMO2 and Polar MM5 (not shown), because of the higher RACMO2 spatial resolution, its data are used henceforth in this reconstruction effort and not the Polar MM5.

The average accumulation for the 1600–2009 period is 698 Gt yr^{-1}. One standard deviation of the annual (11-yr smoothed) data is 111 Gt yr^{-1} (54 Gt yr^{-1}). Vernon et al. (2012) compare surface mass balance components among several regional climate models. A key source of disagreement among the models is differing assignment of the land surface classification (or land use) masks of ice, land, or water. For example, this reconstruction in the 1958–2009 period has a 50 Gt yr^{-1} larger accumulation than Ettema et al. (2009), who calculate 697 Gt yr^{-1}. This discrepancy underscores the need for a common mask used by the science community.

c. Calibration

The ability of the reconstruction to reproduce whole ice sheet annual total accumulation is checked by comparing $\hat{A}_t(G)$ values versus the RCM output upon which the regression is based (Fig. 5a). The reconstructed values exhibit a significant correlation ($R = 0.727$, $1 - p > 0.999$) but have a lower interannual range of values.

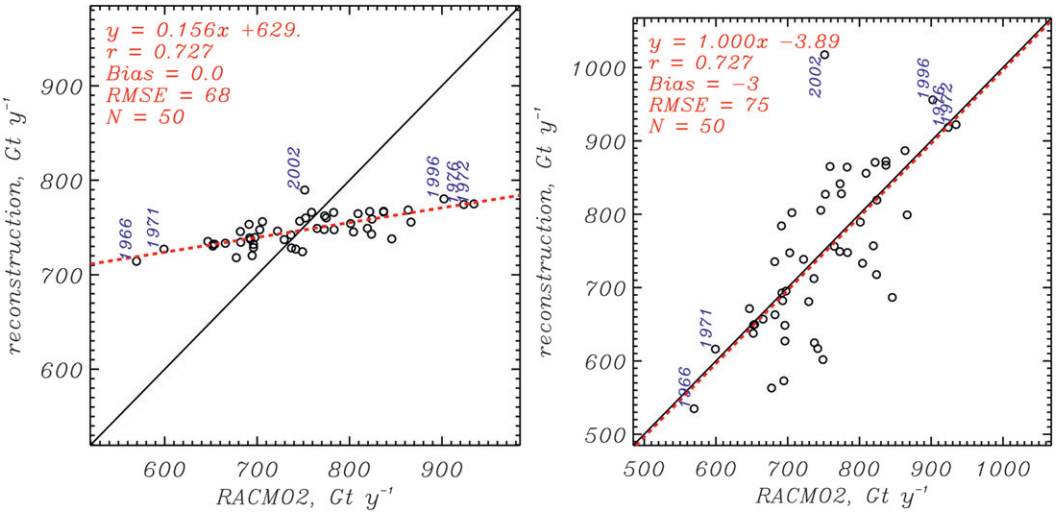

FIG. 5. (left) Comparison of Greenland ice sheet annual total net snow accumulation for our statistical reconstruction vs the RACMO2 regional climate model output. The least squares regression fit is indicated by the red dashed line. Years with accumulation rate exceeding 1.5 standard deviations from the RACMO2 mean are annotated with blue text. Year 2002, anomalously large for the reconstruction, is also annotated. (right) As at left, but with regression effect compensated using the regression function (left). These data are not smoothed temporally.

Least squares regression is accurate in reproducing the average of a dependent variable. It is, however, by construction, limited in reproducing the observed range of extreme values. The calibration factor indicates the need to reassign an amplitude increase by a factor of more than 6 because of this *regression effect*. The regression effect is to be expected because we are estimating the mean annual accumulation without accounting fully or directly for the year-to-year variability of the true accumulation $\hat{A}_t(G)$. Compensating for the regression effect is straightforward using the regression-fitted slope and intercept to reamplify estimated accumulation values. By design, this amplitude coefficient, 6.38, produces an interannual range of values that is in agreement with that of RACMO2 (Fig. 5b). A correspondence between the anomalously high accumulation years (1972, 1976, and 1996) and the anomalously low accumulation years (1971 and 1966) is evident between the RACMO2 data and the reconstruction. However, the reconstruction overpredicts year 2002's accumulation because southeast Greenland cores are more common late in the reconstruction where the 2002 anomalously high accumulation occurred (Box et al. 2005).

5. Results and discussion

a. Temporal variability

Strong interdecadal cyclicity of whole ice sheet accumulation rate are evident in $\hat{A}_t(G)$ (Fig. 6). These are similar to ACR_t ($R = 0.533, 1 - p > 0.999$). The similarity is not surprising given that $\hat{A}_t(G)$ incorporates the same five cores as ACR_t in addition to others. While ACR_t data do not indicate long-term trends by design, examples of four possible $\hat{A}_t(G)$ trend periods are set, either arbitrarily (1600–2009, 1700–2009, 1800–2009, and 1900–2009) or from select periods identified by visual estimation of the time series as increasing (1840–2009, 1840–1945, and 1964–2009) or decreasing (1945–68). Over the full 410-yr period of the reconstruction, 1600–2009, a significant 12% increase (124 Gt yr^{-1}) in accumulation rate is evident (Table 2). Relatively strong changes are evident, for example in the periods 1945–68 and 1968–96. There is some evidence of an increasing accumulation rate trend (an acceleration) after the trendless 1800s (Fig. 6, Table 2). The 1840–1996 trend is 30% higher than the 1600–2009 trend.

b. Periodic variability

Before the regional source of the apparent trends is considered, the apparent interdecadal cyclicity is examined using a Morlet wavelet analysis (Torrence and Compo 1998) sensitive to periodicity and its possible temporal variability. An ~30-yr cyclicity around year ~1700 that decreases to under 20 yr after year 1850 is evident in both ACR_t and $\hat{A}_t(G)$ (Figs. 7a,b). Another cyclicity is consistent among the two time series before 1800, centered at ~12 yr. Shorter-period cyclicity is also evident in $\hat{A}_t(G)$ at this time because the $\hat{A}_t(G)$ values have annual resolution, whereas this signal is not evident in ACR_t since it is based on a 10-yr running statistic. Cyclicity in the interdecadal variations of $\hat{A}_t(G)$ suggests

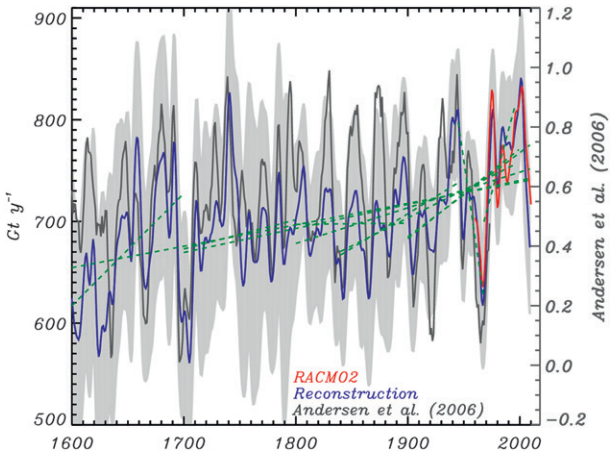

FIG. 6. Time series of total Greenland ice sheet snow accumulation based on the RACMO2 regional climate model and our statistical reconstruction. The annual reconstruction totals are smoothed with an 11-yr Gaussian filter to emphasize interdecadal variations. A light gray area indicates the 1.28σ uncertainty envelope corresponding to 80% confidence. Green dashed lines indicate trend fits for a selection of periods (see Table 3) based on the unsmoothed totals. The right vertical axis is for the Andersen et al. (2006) data, which are normalized, offering values between zero and 1.

TABLE 2. Whole ice sheet accumulation rate trend statistics.

Arbitrary century	Number of years	Change, Gt	Change, %	Confidence, %
1600–99	100	110	16	74.3
1700–99	100	29	4	75.1
1800–99	100	1	0	41.9
1900–99	100	88	12	89.2
Arbitrary period				
1600–2009	410	86	12	95.3
1700–2009	310	73	10	90.8
1800–2009	210	74	10	91.7
1900–2009	110	91	12	90.0
Select period				
1840–1945	106	72	10	68.0
1945–68	24	−180	−25	82.9
1968–96	29	119	16	73.1
1840–1996	157	86	12	90.5

the influence of an atmospheric teleconnection such as the NAO, discussed later.

c. *Spatiotemporal variability in the reconstruction*

According to linear regression, the greatest long-term changes in estimated accumulation $\hat{\mu}_t(s)$ occur in southeastern Greenland (Fig. 8a). The change relative to the average over that period reveals a complementary picture (Fig. 8b). Since 1840, coinciding roughly with the end of the Little Ice Age, $\Delta\hat{A}_t(G)$ increases are widespread in northern, southwestern, and southeastern areas. The 1945–68 overall decline (Fig. 6) is concentrated east of the topographic divide and is accompanied by net increases across the northwestern ice sheet (not shown). Examining several different trend periods (not shown), the sign of $\Delta\hat{A}_t(G)$ alternates along the east–west axis of the ice sheet topographic divide, which is consistent with earlier findings (e.g., Burgess et al. 2010).

While the localized negative anomaly in $\Delta\hat{A}_t(G)$ at the extreme southeastern ice sheet suggests a complex pattern, it is not a significant change above $(1 - p) = 0.8$. From a strict statistics perspective, Fig. 8 is better thought of as a visualization of accumulation changes over time that may be used for hypothesis generation, rather than providing the ability to infer highly localized

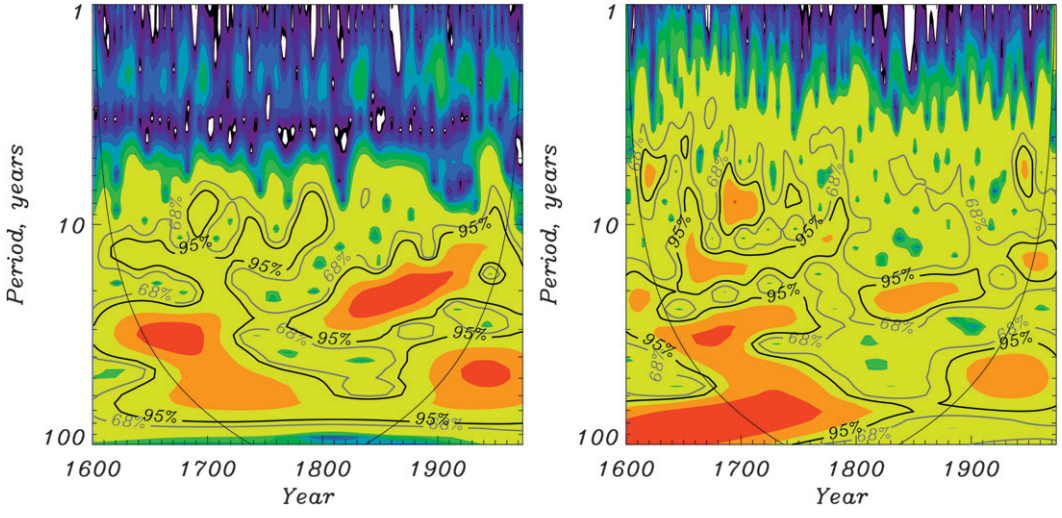

FIG. 7. Local wavelet power spectra of (left) the Andersen et al. (2006) common record {ACRt} and (right) the reconstructed $\hat{A}t(G)$ of this study. Colors represent magnitude of power.

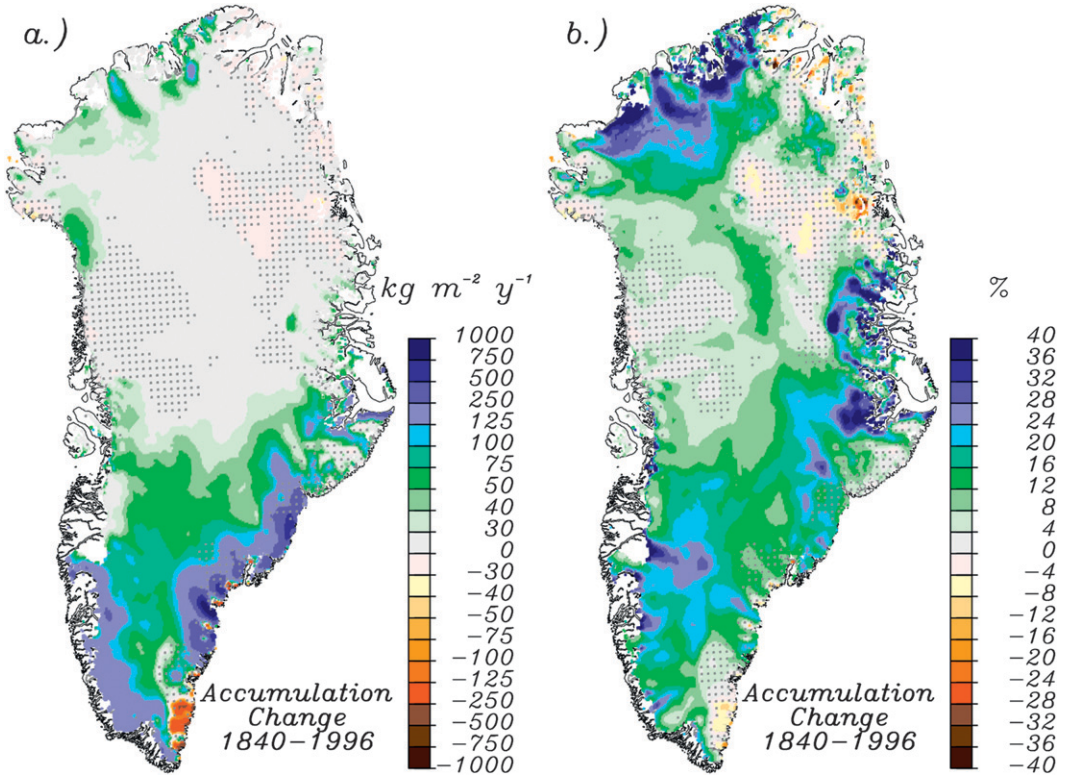

FIG. 8. Spatial patterns of the (a) absolute and (b) percent changes in reconstructed ice sheet accumulation rate from 1840 to 1996. Nonstippled areas have trends associated with a confidence exceeding 80%.

spatial changes. One should not read too much into the detail of the maps because of the issue of spatial dependence, and this is technically not a spatial statistical reconstruction model.

d. Regional correlation

In the 121-yr period of common overlap (1880–2005) between $\hat{A}_t(G)$ and a number of other regional climate data series, colinear variability correlations suggest climate interactions (Fig. 9). In the 1880–1939 period, $\hat{A}_t(G)$ is found to correlate, in absolute value, in excess of 0.65 with winter North Atlantic Oscillation (NAO:DJFM$_t$), North Atlantic SST (SSTNA$_t$), and Northern Hemisphere near surface air temperature (SATNH$_t$) but not with local Greenland ice sheet near-surface temperature (SATG$_t$) after the Box et al. (2009) reconstruction

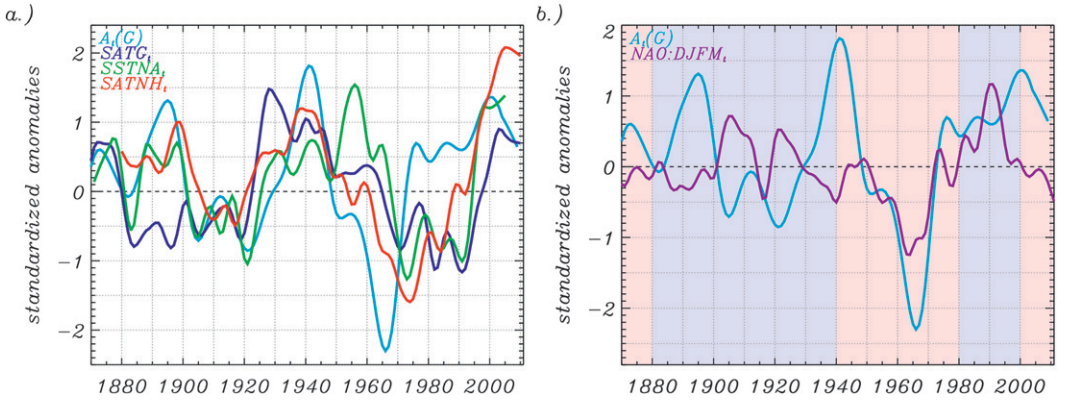

FIG. 9. Comparison of Greenland ice sheet accumulation rates with near-surface air or sea surface temperature time series. All time series are smoothed with an 11-yr Gaussian running average, and they are temporally detrended and standardized over the 1880–2005 period.

TABLE 3. Correlation between Greenland ice sheet accumulation rate and regional climate parameters. Bold (italicized) values correspond to the 1880–1939 (1940–80) period.

Variable	$\hat{A}_t(G)$	$SATG_t$	$NAO{:}DJFM_t$	$SSTNA_t$	$SATNH_t$
$\hat{A}_t(G)$	—	**0.040**	**−0.708**	**0.789**	**0.652**
$SATG_t$	*0.470*	—	**−0.116**	**0.335**	**0.416**
$NAO{:}DJFM_t$	*0.754*	*0.077*	—	**−0.716**	**−0.443**
$SSTNA_t$	*−0.076*	*0.691*	*−0.318*	—	**0.666**
$SATNH_t$	*0.488*	*0.932*	*0.157*	*0.689*	—

(Table 3). In the subsequent 1940–80 period, the absolute value of the correlation of $\hat{A}_t(G)$ with $NAO{:}DJFM_t$ remains high but flips in sign. We find a strong negative correlation between $\hat{A}_t(G)$ and $NAO{:}DJFM_t$ in the 60-yr period, 1880–1939, which can be compared to a strong *positive* correlation in the 41 yr spanning 1940–80. The sign of the correlation of $NAO{:}DJFM_t$ with $\hat{A}_t(G)$ reverses four times in the 1880–2005 period, as illustrated by shaded areas in Fig. 9b. We do not find a clear explanation for the flip in correlation between 1880–1980, even after examining composites in mean sea level pressure and 500-hPa geopotential heights for extreme positive and negative NAO values (not shown).

In this period, a correlation above 0.47 with $SATNH_t$ is maintained, and a positive $SATG_t$ correlation is observed (Table 3). It is clear that multidecadal phase differences (Fig. 9a) degrade these correlations. For example, $SATG_t$ leads $\hat{A}_t(G)$ by approximately 10 yr in the 1920s; then $\hat{A}_t(G)$ leads $SATG_t$ by approximately 20 yr after 1960. Correlations tend to increase with averaging interval as the influence of phase differences is damped.

Incidentally, the $SATG_t$ versus $SSTNA_t$ or $SATNH_t$ correlations remain positive over this 101-yr (1880–1980) period and $SSTNA_t$ consistently correlates highly with $SATNH_t$. A consistent negative correlation between $NAO{:}DJFM_t$ and $SSTNA_t$ is evident.

e. Temperature sensitivity

Numerous studies find some evidence of an increase in Arctic precipitation rates with increasing air temperatures. A twentieth-century Arctic-wide precipitation increase of ~1% decade^{-1} is reproduced by observationally constrained model simulations of twentieth-century climate (Kattsov and Walsh 2000; Paeth et al. 2002). There is evidence in these studies of the largest increase occurring from the 1920s to the 1940s, a period that is marked by ice sheet warming (Box et al. 2009). Our reconstruction contains an equivalent rate of increase for the twentieth century (1.2% decade^{-1}); see 1900–99 in Table 2 and a relatively large increase between 1920 and 1940. The values of $\hat{A}_t(G)$ reach a century-scale minimum at a time that roughly coincides with relatively low air temperatures at the end of the Little Ice Age (LIA) in Greenland (Dahl-Jensen et al. 1998). Paeth et al. (2002) link the increasing precipitation to increasing SST and atmospheric CO_2. Model projections described in the Arctic Climate Impact Assessment (ACIA 2005) lead to expectations of increases in precipitation minus evaporation (accumulation) between 1981–2000 and 2071–90 in all terrestrial (+6% to +12%) and oceanic (+14%) regions.

Regarding the explicit accumulation sensitivity to air temperature, Gregory and Oerlemans (1998) simulate for Greenland a 3% K^{-1} precipitation sensitivity in a future hemispheric warming scenario. Our $\hat{A}_t(G)$ and Northern Hemisphere near-surface air temperatures from NASA Goddard Institute for Space Studies (GISS), with and without temporal detrending, yields a consistent sensitivity of 6.8% K^{-1} or 51 Gt K^{-1} (correlation = 0.804, $1 - p > 0.999$, N yr = 82; 1880–1962). This result does not mean that high temperatures *cause* high accumulation through the Clausius–Clapeyron effect locally. In fact, the correlation of $\hat{A}_t(G)$ with local ice sheet temperatures after Box et al. (2009) is low. The implication is that the nonzero and positive accumulation sensitivity to Northern Hemisphere near-surface air temperatures are connected via the advection of distant air masses that contain more moisture in a warmer hemispheric environment.

6. Conclusions

Long-term Greenland ice sheet accumulation rate reconstruction is enabled by combining available ice core records and independent regional climate model outputs in ways that exploit their respective strengths in temporal and spatial coverage. While Polar MM5 produces similar spatial patterns of accumulation with ice cores as does RACMO2, the latter is used to represent the spatial distribution of accumulation rates because of its higher spatial resolution.

The correlation between ice cores and regional climate model gridded accumulation rates exhibits distinct distance–decay patterns and antiphase correlation patterns across topographic divides.

Our reconstruction suggests that since the 1600s, Greenland ice sheet accumulation rates have increased. The estimated mean accumulation rate in the most recent 170 years (1840–2009) is 30% greater than the estimated mean accumulation rate in the 410 years since 1600, suggesting an acceleration in accumulation rate.

The correlation of reconstructed accumulation rates with the Northern Hemisphere average surface air temperature

remains positive through time, while the correlation with local near-surface air temperatures or North Atlantic sea surface temperatures is inconsistent over time, suggesting a larger-scale, hemispheric-scale climate connection.

The reconstructed accumulation rate correlates consistently highly with the North Atlantic Oscillation index. Yet, the sign of this correlation flips four times in the 1870–2005 period. The cause of this fluctuation in correlation remains unexplained.

The ice sheet accumulation rate exhibits positive correlations with Northern Hemispheric near-surface air temperatures. The climate sensitivity we derive suggests that average annual accumulation rate increases with Northern Hemispheric near-surface air temperature by 6.8% K^{-1} or 51 Gt K^{-1}.

The ice sheet reconstructed accumulation rates from this study spanning 1600–2009 are posted with annual and 11-yr Gaussian smoothed temporal resolutions online at http://bprc.osu.edu/wiki/Greenland_Accumulation_Grids.

Acknowledgments. This work was supported by the Cryospheric Sciences Program of NASA's Earth Science Enterprise Grants NNG04GH70G and NNX07AM82G and The Ohio State University's Climate Water Carbon initiative. ACT-10 and ACT-11 cores were obtained with the support of National Science Foundation Office of Polar Programs Award ARC-090946 and ARC-0909499 managed by H. Edmonds and made possible by the American Recovery and Reinvestment Act of 2009. E. Burgess assisted in ACT-10 and ACT-11 field work and planning. Professor Cressie's research was supported by the SSES Program at The Ohio State University. M. van den Broeke and J. van Angelen acknowledge support from the Netherlands Polar Program and the EU FP7 project ice2sea. The Humboldt, Tunu-N, and NEEM-08 ice core records were developed under NSF Grant 0909541 and the Summit-Zoe-10 record under NSF Grant 0856845. We gratefully acknowledge the contributions of field and laboratory personnel in obtaining all the ice core records used in this study.

REFERENCES

ACIA, 2005: *Arctic Climate Impact Assessment.* Cambridge University Press, 1042 pp.

Aðalgeirsdóttir, G., M. Stendel, J. H. Christensen, J. Cappelen, F. Vejen, H. A. Kjær, R. H. Mottram, and P. Lucas-Picher, 2009: Assessment of the temperature, precipitation and snow in the RCM HIRHAM4 at 25 km resolution. Climate Center Rep. 09-08, Danish Meteorological Institute, 80 pp. [Available online at http://www.dmi.dk/dmi/dkc09-08.pdf.]

Andersen, K. K., P. D. Ditlevsen, S. O. Rasmussen, H. B. Clausen, B. M. Vinther, S. J. Johnson, and J. P. Steffensen, 2006: Retrieving a common accumulation record from Greenland ice cores for the past 1800 years. *J. Geophys. Res.,* **111,** D15106, doi:10.1029/2005JD006765.

Bales, R. C., J. R. McConnell, E. Mosley-Thompson, and B. Csatho, 2001a: Accumulation over the Greenland ice sheet from historical and recent records. *J. Geophys. Res.,* **106,** 33 813–33 825.

——, E. Mosley-Thompson, and J. R. McConnell, 2001b: Variability of accumulation in northwest Greenland over the past 250 years. *Geophys. Res. Lett.,* **28,** 2679–2682.

——, and Coauthors, 2009: Annual accumulation for Greenland updated using ice core data developed during 2000–2006 and analysis of daily coastal meteorological data. *J. Geophys. Res.,* **114,** D06116, doi:10.1029/2008JD011208.

Banta, J. R., and J. R. McConnell, 2007: Annual accumulation over recent centuries at four sites in central Greenland. *J. Geophys. Res.,* **112,** D10114, doi:10.1029/2006JD007887.

——, ——, R. Edwards, and J. P. Engelbrecht, 2008: Delineation of carbonate dust, aluminous dust, and sea salt deposition in a Greenland glaciochemical array using positive matrix factorization. *Geochem. Geophys. Geosyst.,* **9,** Q07013, doi:10.1029/2007GC001908.

Box, J. E., 2005: Greenland ice sheet surface mass balance variability: 1991–2003. *Ann. Glaciol.,* **42,** 90–94.

——, and K. Steffen, 2001: Sublimation on the Greenland ice sheet from automated weather station observations. *J. Geophys. Res.,* **106,** 33 965–33 982.

——, and A. Rinke, 2003: Evaluation of Greenland ice sheet surface climate in the HIRHAM regional climate model. *J. Climate,* **16,** 1302–1319.

——, D. H. Bromwich, and L.-S. Bai, 2004: Greenland ice sheet surface mass balance for 1991–2000: Application of Polar MM5 mesoscale model and in situ data. *J. Geophys. Res.,* **109,** D16105, doi:10.1029/2003JD004451.

——, L. Yang, J. Rogers, D. Bromwich, L.-S. Bai, K. Steffen, J. C. Stroeve, and S.-H. Wang, 2005: Extreme precipitation events over Greenland: Consequences to ice sheet mass balance. *Extended Abstracts, Eighth Conf. on Polar Meteorology and Oceanography,* San Diego, CA, Amer. Meteor. Soc., 5.2. [Available online at https://ams.confex.com/ams/Annual2005/techprogram/paper_87528.htm.]

——, and Coauthors, 2006: Greenland ice sheet surface mass balance variability (1988–2004) from calibrated Polar MM5 output. *J. Climate,* **19,** 2783–2800.

——, L. Yang, D. H. Bromwich, and L.-S. Bai, 2009: Greenland ice sheet surface air temperature variability: 1840–2007. *J. Climate,* **22,** 4029–4049.

Bromwich, D. H., J. Cassano, T. Klein, G. Heinemann, K. Hines, K. Steffen, and J. E. Box, 2001: Mesoscale modeling of katabatic winds over Greenland with the Polar MM5. *Mon. Wea. Rev.,* **129,** 2290–2309.

Burgess, E. W., R. R. Forster, J. E. Box, E. Mosley-Thompson, D. H. Bromwich, R. C. Bales, and L. C. Smith, 2010: A spatially calibrated model of annual accumulation rate on the Greenland Ice Sheet (1958–2007). *J. Geophys. Res.,* **115,** F02004, doi:10.1029/2009JF001293.

Calanca, P., H. Gilgen, S. Ekholm, and A. Ohmura, 2000: Gridded temperature and accumulation distributions for Greenland for use in cryospheric models. *Ann. Glaciol.,* **31,** 118–120, doi:10.3189/172756400781820345.

Cassano, J., J. E. Box, D. H. Bromwich, L. Li, and K. Steffen, 2001: Verification of Polar MM5 simulations of Greenland's atmospheric circulation. *J. Geophys. Res.,* **106,** 33 867–33 890.

Chen, Q., D. H. Bromwich, and L. Bai, 1997: Precipitation over Greenland retrieved by a dynamic method and its relation to cyclonic activity. *J. Climate,* **10,** 839–870.

Clausen, H. B., and C. U. Hammer, 1988: The Laki and Tambora eruptions as revealed in Greenland ice cores from 11 locations. *Ann. Glaciol.,* **10,** 16–22.

——, N. S. Gundestrup, and S. J. Johnsen, 1988: Glaciological investigations in the Crête area, central Greenland: A search for a new deep-drilling site. *Ann. Glaciol.,* **10,** 10–15.

Cogley, J. G., 2004: Greenland accumulation: An error model. *J. Geophys. Res.,* **109,** D18101, doi:10.1029/2003JD004449.

Dahl-Jensen, D., K. Mosegaard, N. Gundestrup, G. D. Clow, S. J. Johnsen, A. W. Hansen, and N. Balling, 1998: Past temperatures directly from the Greenland ice sheet. *Science,* **282,** 268–271.

Déry, S. J., and M. K. Yau, 1999: A bulk blowing snow model. *Bound.-Layer Meteor.,* **93,** 237–251.

Dethloff, K., and Coauthors, 2002: Recent Greenland accumulation estimated from regional climate model simulations and ice core analysis. *J. Climate,* **15,** 2821–2832.

Ettema, J., M. R. van den Broeke, E. van Meijgaard, W. J. van de Berg, J. L. Bamber, J. E. Box, and R. C. Bales, 2009: Higher surface mass balance of the Greenland Ice Sheet revealed by high-resolution climate modeling. *Geophys. Res. Lett.,* **36,** L12501, doi:10.1029/2009GL038110.

Fettweis, X., E. Hanna, H. Gallée, P. Huybrechts, and M. Erpicum, 2008: Estimation of the Greenland ice sheet surface mass balance for the 20th and 21st centuries. *Cryosphere,* **2,** 117–129.

Forster, R. R., C. Miege, J. E. Box, J. R. McConnell, V. B. Spikes, and E. W. Burgess, 2010: Arctic Circle Traverse 2010 (ACT-10): SE Greenland snow accumulation variability from firn coring and ice sounding radar. *Proc. Fall AGU Meeting,* San Francisco, CA, Amer. Geophys. Union, Abstract C13B-0554.

Gregory, J. M., and J. Oerlemans, 1998: Simulated future sea-level rise due to glacier melt based on regionally and seasonally resolved temperature changes. *Nature,* **391,** 474–476.

Hanna, E., P. Valdes, and J. McConnell, 2001: Patterns and variations of snow accumulation over Greenland, 1979–98, from ECMWF analyses, and their verification. *J. Climate,* **14,** 3521–3535.

——, P. Huybrechts, I. Janssens, J. Cappelen, K. Steffen, and A. Stephens, 2005: Runoff and mass balance of the Greenland ice sheet: 1958–2003. *J. Geophys. Res.,* **110,** D13108, doi:10.1029/2004JD005641.

——, J. McConnell, S. Das, J. Cappelen, and A. Stephens, 2006: Observed and modelled Greenland Ice Sheet snow accumulation, 1958–2003, and links with regional climate forcing. *J. Climate,* **19,** 344–358.

——, and Coauthors, 2011: Greenland Ice Sheet surface mass balance 1870 to 2010 based on twentieth century reanalysis, and links with global climate forcing. *J. Geophys. Res.,* **116,** D24121, doi:10.1029/2011JD016387.

Hansen, J., R. Ruedy, J. Glascoe, and M. Sato, 1999: GISS analysis of surface temperature change. *J. Geophys. Res.,* **104,** 30 997–31 022.

——, ——, M. Sato, and K. Lo, 2010: Global surface temperature change. *Rev. Geophys.,* **48,** RG4004, doi:10.1029/2010RG000345.

Hurrell, J. W., 1995: Decadal trends in the North Atlantic Oscillation regional temperatures and precipitation. *Science,* **269,** 676–679.

Hutterli, M. A., C. C. Raible, and T. F. Stocker, 2005: Reconstructing climate variability from Greenland ice sheet accumulation: An ERA40 study. *Geophys. Res. Lett.,* **32,** L23712, doi:10.1029/2005GL024745.

Kargel, J. S., and Coauthors, 2011: Greenland's shrinking ice cover: ''Fast times'' but not that fast. *Cryosphere,* **5,** 3207–3219, doi:10.5194/tcd-5-3207-2011.

Kattsov, V. M., and J. E. Walsh, 2000: Twentieth-century trends of Arctic precipitation from observational data and a climate model simulation. *J. Climate,* **13,** 1362–1370.

Kiilsholm, S., J. H. Christensen, K. Dethloff, and A. Rinke, 2003: Net accumulation of the Greenland ice sheet: High resolution modeling of climate changes. *Geophys. Res. Lett.,* **30,** 1485, doi:10.1029/2002GL015742.

Lenaerts, J. T. M., and M. R. van den Broeke, 2012: Modeling drifting snow in Antarctica with a regional climate model: 2. Results. *J. Geophys. Res.,* **117,** D05109, doi:10.1029/2010JD015419.

——, ——, S. J. Déry, G. König-Langlo, J. Ettema, and P. K. Munneke, 2010: Modelling snowdrift sublimation on an Antarctic ice shelf. *Cryosphere,* **4,** 179–190.

——, ——, J. H. van Angelen, E. van Meijgaard, and S. J. Déry, 2012a: Drifting snow climate of the Greenland ice sheet: A study with a regional climate model. *Cryosphere,* **6,** 891–899, doi:10.5194/tc-6-891-2012.

——, ——, W. J. van de Berg, E. van Meijgaard, and P. Kuipers Munneke, 2012b: A new, high-resolution surface mass balance map of Antarctica (1979–2010) based on regional atmospheric climate modeling. *Geophys. Res. Lett.,* **39,** L04501, doi:10.1029/2011GL050713.

Lucas-Picher, P., M. Wulff-Nielsen, J. H. Christensen, G. Aðalgeirsdóttir, R. H. Mottram, and S. B. Simonsen, 2011: Very high resolution regional climate model simulations over Greenland identifying added value. *J. Geophys. Res.,* **117,** D02108, doi:10.1029/2011JD016267.

Mayewski, P. A., W. B. Lyons, M. J. Spencer, M. S. Twickler, C. F. Buck, and S. Whitlow, 1990: An ice-core record of atmospheric response to anthropogenic sulphate and nitrate. *Nature,* **346,** 554–556.

McConnell, J. R., E. Mosley-Thompson, D. H. Bromwich, R. C. Bales, and J. Kyne, 2000: Interannual variations of snow accumulation on the Greenland Ice Sheet (1985–1996): New observations versus model predictions. *J. Geophys. Res.,* **105,** 4039–4046.

——, G. Lamorey, E. Hanna, E. Mosley-Thompson, R. C. Bales, D. Belle-Oudry, and J. D. Kyne, 2001: Annual net snow accumulation over southern Greenland from 1975 to 1998. *J. Geophys. Res.,* **106,** 33 827–33 837.

Mernild, S. H., G. E. Liston, C. A. Hiemstra, and K. Steffen, 2008: Surface melt area and water balance modeling on the Greenland ice sheet 1995–2005. *J. Hydrometeor.,* **9,** 1191–1211.

Mosley-Thompson, E., and Coauthors, 2001: Local to regional-scale variability of annual net accumulation on the Greenland Ice Sheet from PARCA cores. *J. Geophys. Res.,* **106** (D24), 33 839–33 851.

——, C. R. Readinger, P. Craigmile, L. G. Thompson, and C. A. Calder, 2005: Regional sensitivity of Greenland precipitation to NAO variability. *Geophys. Res. Lett.,* **32,** L24707, doi:10.1029/2005GL024776.

Ohmura, A., and N. Reeh, 1991: New precipitation and accumulation maps of Greenland. *J. Glaciol.,* **37,** 140–148.

——, M. Wild, and L. Bengtsson, 1996: A possible change in mass balance of Greenland and Antarctic ice sheets in the coming century. *J. Climate,* **9,** 2124–2135.

Paeth, H., A. Hense, and R. Hagenbrock, 2002: Comments on ''Twentieth century trends of Arctic precipitation from observational data and a climate model simulation.'' *J. Climate,* **15,** 800–803.

Rae, J. G. L., and Coauthors, 2012: Greenland ice sheet surface mass balance: Evaluating simulations and making projections with regional climate models. *Cryosphere,* **6,** 1275–1294, doi:10.5194/tc-6-1275-2012.

Rayner, N. A., P. Brohan, D. E. Parker, C. K. Folland, J. J. Kennedy, M. Vanicek, T. Ansell, and S. F. B. Tett, 2006: Improved analyses of changes and uncertainties in sea surface temperature measured in situ since the mid-nineteenth century: The HadSST2 data set. *J. Climate,* **19,** 446–469.

Rogers, J. C., D. J. Bathke, E. Mosley-Thompson, and S.-H. Wang, 2004: Atmospheric circulation and cyclone frequency variations linked to the primary modes of Greenland snow accumulation. *Geophys. Res. Lett.,* **31,** L23208, doi:10.1029/2004GL021048.

Thompson, S., and D. Pollard, 1997: Greenland and Antarctic mass balances for present and doubled atmospheric CO_2 from the GENESIS version-2 global climate model. *J. Climate,* **10,** 871–900.

Torrence, C., and G. P. Compo, 1998: A practical guide to wavelet analysis. *Bull. Amer. Meteor. Soc.,* **79,** 61–78.

Undén, P., and Coauthors, 2002: HIRLAM-5 scientific documentation. Swedish Meteorological and Hydrological Institute Tech. Rep., 144 pp.

Van Angelen, J. H., M. R. van den Broeke, and W. J. van de Berg, 2011: Momentum budget of the atmospheric boundary layer over the Greenland ice sheet and its surrounding seas. *J. Geophys. Res.,* **116,** D10101, doi:10.1029/2010JD015485.

Van de Berg, W. J., M. R. van den Broeke, C. H. Reijmer, and E. van Meijgaard, 2006: Reassessment of the Antarctic surface mass balance using calibrated output of a regional atmospheric climate model. *J. Geophys. Res.,* **111,** D11104, doi:10.1029/2005JD006495.

Van den Broeke, M. R., and Coauthors, 2009: Partitioning recent Greenland mass loss. *Science,* **326,** 984–986.

Van Meijgaard, E., L. H. van Ulft, W. J. Van de Berg, F. C. Bosvelt, B. J. J. M. Van den Hurk, G. Lenderink, and A. P. Siebesma, 2008: The KNMI regional atmospheric model RACMO version 2.1. KNMI Tech. Rep. 302, 43 pp. [Available online at http://www.knmi.nl/bibliotheek/knmipubTR/TR302.pdf.]

Vernon, C. L., J. L. Bamber, J. E. Box, M. R. van den Broeke, X. Fettweis, E. Hanna, and P. Huybrechts, 2012: Surface mass balance model intercomparison for the Greenland ice sheet. *Cryosphere Discuss.,* **6,** 3999–4036, doi:10.5194/tcd-6-3999-2012.

Vinther, B. M., P. D. Jones, K. R. Briffa, H. B. Clausen, K. K. Andersen, D. Dahl-Jensen, and S. J. Johnsen, 2010: Climatic signals in multiple highly resolved stable isotope records from Greenland. *Quat. Sci. Rev.,* **29,** 522–538.

Wake, L. M., P. Huybrechts, J. E. Box, E. Hanna, I. Janssens, and G. A. Milne, 2009: Surface mass-balance changes of the Greenland ice sheet since 1866. *Ann. Glaciol.,* **50,** 178–184.

Walsh, J. E., W. L. Chapman, V. Romanovsky, J. H. Christensen, and M. Stendel, 2008: Global climate model performance over Alaska and Greenland. *J. Climate,* **21,** 6156–6174.

White, J. W. C., L. K. Barlow, D. Fisher, P. Grootes, J. Jouzel, S. J. Johnsen, M. Stuiver, and H. Clausen, 1997: The climate signal in the stable isotopes of snow from Summit, Greenland: Results of comparisons with modern climate observations. *J. Geophys. Res.,* **102,** 26 425–26 439.

Wild, M., and A. Ohmura, 2000: Change in mass balance of polar ice sheets and sea level from high-resolution GCM simulations of greenhouse warming. *Ann. Glaciol.,* **30,** 197–203.